Mass production of graphene using high-power rapid joule heating method

Dan-Na Wu [a,1], Jian Sheng [b,1], Hai-Gang Lu [a,c,*], Si-Dian Li [a,*], Yan Li [b,*]

[a] *Key Laboratory of Chemical Biology and Molecular Engineering of Ministry of Education, Institute of Molecular Science, Shanxi University, Taiyuan 030006, China*
[b] *Beijing National Laboratory for Molecular Sciences, Key Laboratory for the Physics and Chemistry of Nanodevices, College of Chemistry and Molecular Engineering, Peking University, Beijing 100871, China*
[c] *Saiyin Materials Co., LTD., JinChuangGu, Taiyuan 030051, China*

ABSTRACT

Graphene has a vast market demand in the industrial field, but the high cost and complexity of traditional production methods limit its application. The newly developed flash Joule heating method based on capacitor discharge presents a cost-effective production alternative for graphene, but the batch yield is still limited in gram-scale level. This study presents a high-power rapid Joule heating (RJH) method based on direct current power discharge to enable mass production of graphene. With this high-power RJH system, 100 g of carbon black can be rapidly heated to 3000 °C within mere minutes, promoting its graphitization transformation, thus achieving a substantial increase in graphene production efficiency. Detailed characterizations confirm the successful synthesis of high-quality turbostratic rapid graphene (RG), with production energy consumption of only ~5 kWh kg^{-1} (approximately \$0.5 kg^{-1} based on current energy prices). Therefore, one can theoretically produce 5 tons of graphene per year in the laboratory for industrial applications. Furthermore, by adding boron oxide and melamine as additives, direct mass production of boron, nitrogen, and nitrogen-boron co-doped RGs can be carried out. Doping modifies the local structure of RG, thereby enhancing its hydrophobicity and electrical conductivity. This work is anticipated to significantly accelerate the process of low-cost bulk production of graphene, thereby broadening its industrial applications.

1. Introduction

Graphene, a two-dimensional material with a honeycomb lattice of sp^2-bonded carbon atoms, has garnered significant scientific and industrial attention due to its exceptional electrical, optical, and mechanical properties [1–4]. Heteroatom doping can further modify the electronic states and properties of graphene [5,6], thereby enabling its application in a wide range of fields. Currently, the annual global production of graphene exceeds 23,000 metric tons. Industries are planning to add graphene to products such as tires, concrete, and asphalt to enhance their properties, which are currently hot areas of commercial investment in graphene [7]. Cost-effective mass production is crucial for achieving the large-scale industrial application of graphene [8]. However, traditional graphene production methods, such as chemical vapor deposition [9], reduction of graphene oxide [10], and graphite exfoliation [11–13], are complex and time-consuming, leading to high production costs.

Since 2020, the flash Joule heating (FJH) method has been regarded as an effective approach to convert solid carbon into turbostratic flash graphene in seconds under the combined action of high temperature and electric field [14–17]. In the FJH process, the capacitor tank can discharge instantaneously at approximately 400 V and 1000 A, delivering 400 kW of power to heat a 1.0-g solid carbon sample to over 3000 °C in milliseconds [14]. By 2023, a small-batch automatic FJH system capable of loading 5.7 g of metallurgical coke per batch had been designed, with a production capacity of 1.1 kg of graphene in 1.5 h [18]. Scaling up this automatic FJH system to produce larger batches of graphene requires additional capacitors. For instance, producing 100 g of graphene per batch would necessitate approximately 480 capacitors of 13 mF each, posing significant challenges in terms of equipment volume and safety due to the 500-volt requirement.

Prior to the advent of the FJH method, the rapid Joule heating (RJH) techniques powered by direct current had been rapidly developed and widely applied in various fields, including the graphitization of carbon
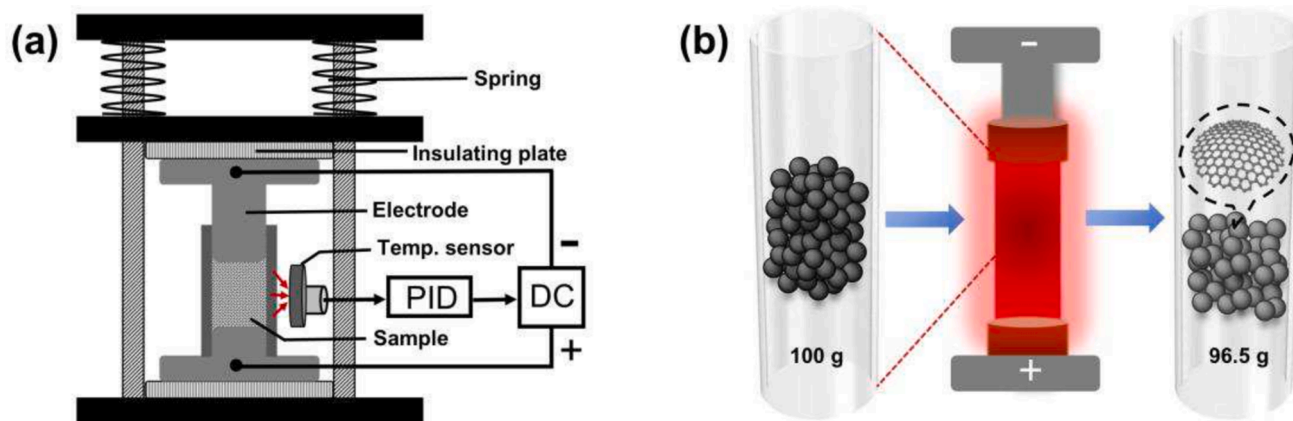
Fig. 1. Schematic of high-power RJH equipment (a) and Joule heating process (b).

fibers [19], the synthesis of high-entropy alloys [20], and the rapid sintering of ceramics [21]. The RJH process has similar advantages to the FJH process, especially in extremely high energy efficiency and ultrafast heating rate. In particular, the equipment cost of the RJH process is lower than that of the FJH process. Compared to the high-power output of 400 kW in the FJH method, previously reported RJH method operates with a power supply of no more than 3 kW in the laboratory but can sustain discharges ranging from microseconds to hours. By increasing the power, the RJH method can heat a large batch of samples to a high temperature of 3000 °C, thereby enabling a process akin to FJH in converting solid carbon sources into graphene.

Here, we demonstrate a high-power RJH system that aims to directly convert 100 g of carbon black into graphene in one batch, making graphene production more efficient, energy-saving, and cost-effective. By adding boron oxide and melamine additives to the carbon black, we can mass-produce heteroatom-doped graphene directly and further investigate the effects of these additives on the crystal structure, hydrophobicity, and conductivity of the generated graphene. The RJH system introduced in this work has the potential to unlock new avenues for the large-scale production of graphene.

2. Experimental

2.1. Graphene production

The raw material chosen for graphene production is conductive carbon black, which possesses properties of high carbon content (>98 %) and low volatility. The used carbon black, which was of the HCD-5 type, was purchased from Tianjin Huacai Co. The additives, melamine (≥99.5 %) and boric oxide (≥99 %), were purchased from Tianjin Kemio Chemical Reagent Co. and Shanghai Hongri Chemical Co., respectively. In order to prevent dusting of carbon black during the RJH process, carbon black, water, and any required additives were uniformly mixed and processed into granules with diameters of 3 mm using a double-roller granulator, followed by drying.

The high-power rapid Joule heating processes were performed using the SaiYin scale-up Joule heating system from Saiyin Materials Co. (Fig. 1a). This system is powered by a 40 kW direct current (DC) power supply, which can deliver output currents ranging from 0 A to 400 A and voltages ranging from 0 V to 100 V. It is also equipped with a Siemens programmable logic controller (PLC), a vacuum box, and an infrared radiation (IR) temperature sensor that can measure temperatures ranging from 400 °C to 3600 °C. The IR temperature sensor is the IRTD-3600LS model (Hangzhou Shanghu Co.). It operates by measuring the intensity of infrared light emitted from blackbody radiation at a wavelength of 1.6 μm, allowing for accurate determination of the temperature. More than 93 % of the infrared light at 1.6 μm is capable of

transmitting through a quartz tube (Fig. S1), thus ensuring reliable and precise temperature measurements.

The sample was placed in a vertical quartz tube secured on a sample holder by two graphite electrodes (Figs. 1b and S2). The quartz tube used for the 100 g sample had an inner diameter of 55 mm, an outer diameter of 65 mm, and a length of 200 mm. Two graphite electrodes with a diameter of 54 mm were used to connect and compress the sample grains. To ensure the sample powder maintains good conductivity during heating, the upper electrode (presumably referring to one of the graphite electrodes used for compression) is pressed tightly by four springs. Additionally, the sample holder is placed on insulating plates to ensure safety during discharge.

Under mild vacuum conditions (about −0.098 MPa), carbon black grains were slightly compressed in the quartz tube, resulting in a sample column with an electric resistance of less than 5 Ω. The amount of carbon black per batch, which is 100 g, exceeds the previously reported maximum weight by ~17.5 times [18]. Throughout the entire Joule heating process, the temperature signal was monitored in real-time by the temperature sensor and transmitted to the PLC's PID (Proportional-Integral-Derivative) controller. The controller adjusts the output voltage and current of the power supply to manage the heating, maintaining, as well as cooling phases, ensuring that the maximum temperature can be maintained at approximately 3000 °C for 5 s. After natural cooling, the graphene is obtained for further investigation.

2.2. Characterizations

Raman spectra from eight randomly selected points on each sample were obtained using a Horiba Jobin-Yvon LabRAM ARAMIS system with a 532 nm wavelength laser. XRD patterns of samples were collected on a Rigaku D/Max-RB, with a 2θ range between 10° and 80°, at room temperature. Transmission electron microscopy (TEM) images were collected using a JEM-2100F instrument operated at 200 kV. Scanning electron microscopy (SEM) using a ZEISS GeminiSEM 300 system at 3 kV with a working distance of 6.6 mm. All samples were sonicated for 15 min and dispersed in an ethanol solution prior to their analysis. X-ray Photoelectron Spectroscopy (XPS) data were collected using a Thermo Scientific K-Alpha instrument.

Contact angle measurements were conducted using a JY-82C instrument. Due to the sample's good water absorption and rapid droplet uptake, video recording was employed to capture images every 62 ms. The image capturing the droplet just as it came into contact with the sample was used to measure the contact angle. Powder resistivity data were obtained using a semiconductor powder resistivity tester (DC-4). The powder sample was evenly distributed in the sample tank, and the resistivity value was recorded at a pressure of 10 MPa.
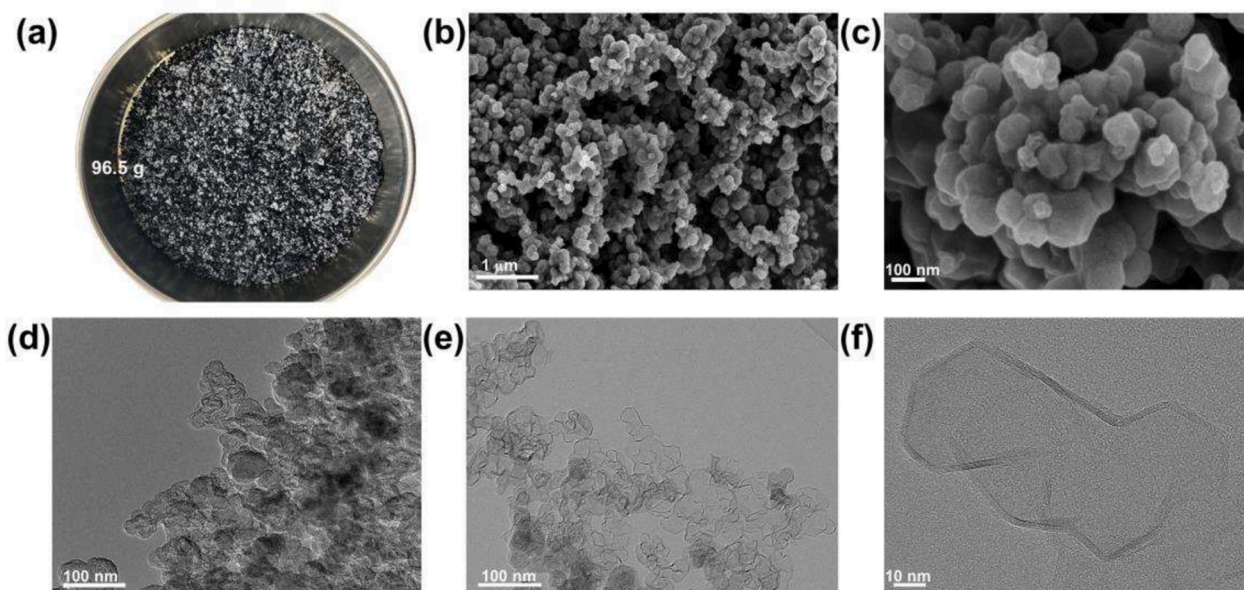
Fig. 2. Photo of graphene grains prepared from conductive carbon black using RJH process (a), SEM images of product with scale bars of 1 μm (b) and 100 nm (c), TEM image of carbon black (d), and TEM images of product with scale bars of 100 nm (e) and 10 nm (f), respectively.
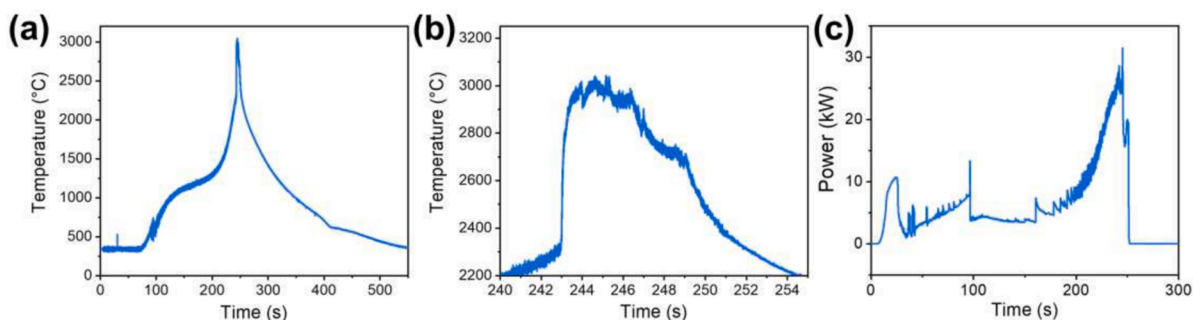

Fig. 3. Temperature profile of the whole RJH process (a) and the graphitization process (b), as well as its power profile (c).

3. Results and discussion

3.1. RJH process for graphene production

After being graphitized at 3000 °C for 5 s, about 96.5 g of graphene powder was obtained. The powder exhibited black and gray colors (Fig. 2a), similar to the appearance of flash graphene [14]. The SEM images show uniform particles of about 100 nm clustered loosely together (see Fig. 2b and c). TEM images show that the amorphous carbon atoms in carbon black (Fig. 2d) have rearranged to produce the wrinkled gauzy morphology (Fig. 2e), consisting of few-layered graphene with sizes of several tens of nanometers (Fig. 2f). The change in microscopic morphology originates from the local transformation of some non-sp^2-carbon to sp^2-carbon, so that the proportion of sp^2-carbon atoms increased from 76.1 % to 84.9 % (Fig. S3). The wrinkled gauzy morphology of the product is similar to the high macro-porosity observed in the molecular simulation of low-density carbon black at 3000 K (Fig. 3d in Ref. [14]).

The temperature profile during the Joule heating process, including heating to 3000 °C, maintaining at 3000 °C, and cooling to 400 °C, is depicted in Fig. 3a. The corresponding voltage, current, and resistance are presented in Fig. S4. By analyzing the temperature curve trends, the RJH process can be divided into pre-heating (<2300 °C) and graphitization (>2300 °C) phases [22]. In the pre-heating stage, the current was less than 50 A due to the high resistance of carbon black grains, and the

sample took about 243 s to heat up gradually from room temperature to 2300 °C. The release of gas caused the sample to become less compact, resulting in an increase in resistance. Subsequently, the compressed springs gradually pushed the upper graphite electrode to descend, maintaining tight contact between the carbon black grains. In the subsequent graphitization process, the sample was rapidly heated to 3000 °C within 1 s, accompanied by a peak discharge current of 320 A (Fig. 3b and S4). Once the PLC controller's PID program adjusted the discharge current to maintain 3000 °C for 5 s, the power was turned off, and the sample began to cool gradually to room temperature. Both heating and cooling rates of the Joule heating method are significantly higher than those of traditional muffle furnaces, justifying the use of the term "rapid" in the rapid Joule heating process.

In this RJH process, the maximum heating power is up to 32 kW (Fig. 3c), significantly less than the 400 kW of the FJH method but much higher than general RJH methods (<1 kW) [20,21]. Therefore, the Saiyin scale-up Joule heating system provides a high-power RJH solution for graphitizing conductive carbon sources. The estimated energy consumption for the RJH production of graphene is ~5 kWh kg^{-1} (approximately \$0.5 kg^{-1} based on current energy prices). The entire heating and cooling process takes roughly 10 min, enabling a total of 144 production cycles within 24 h, resulting in the production of over 13.9 kg of graphene, i.e. about 5.0 tons per year. To the best of our knowledge, producing a nearly 100 g graphene per batch in approximately ten minutes surpasses the capabilities of the other laboratory
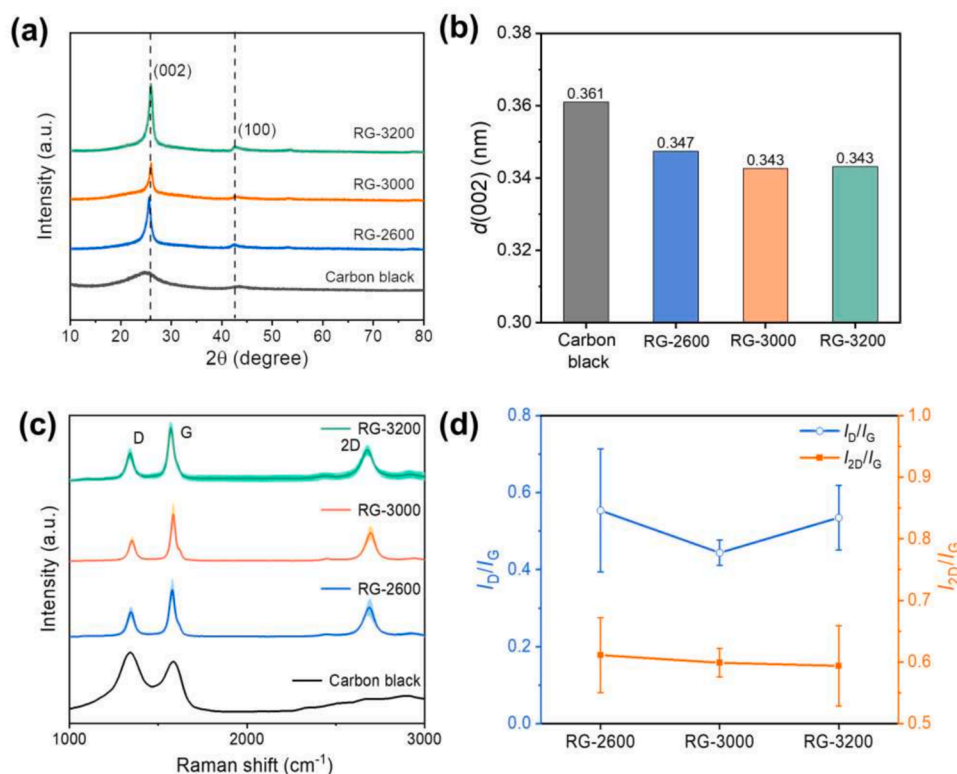
Fig. 4. XRD patterns (a), d(0 0 2) interlayer distances (b), Raman spectra (c), and I_D/I_G and I_{2D}/I_G ratios (d) of rapid graphenes, as well as carbon black.

methods, including flash Joule heating method, chemical vapor deposition, reduction of graphene oxide, and graphite exfoliation (Table S1). Due to its rapid processing, high temperature, and low energy consumption, the high-power RJH method presents an efficient and viable approach for mass production of graphene, which we denote as rapid graphene (RG).

The RJH process bears similarities to the FJH process in the mechanisms for graphene production, both of which involve high graphitization temperatures around 3000 °C, with the RJH process achieving heating rates of about 1100 °C s^{-1} from 2300 °C to 3000 °C, and cooling rates of about 110 °C s^{-1} from 3000 °C to 2300 °C. The process occurs over a short duration of time, only 5 s, significantly less than the tens of hours required for industrial graphitization. This short period is not enough to align the two-dimensional sheets to stack perfectly in Bernal (AB-stacked) structure. Consequently, this rapid temperature fluctuation results in a highly nonequilibrium thermodynamic process, leading to the formation of the turbostratic structure for graphene.

However, there are notable differences in the setups and suitability between RJH and FJH processes. The RJH process utilizes a DC power supply for continuous power delivery, leading to a slightly slower and more controllable heating rate compared to FJH. This moderate graphitization process offers better control over the production of graphene. Nevertheless, in the laboratory, the RJH requires a special 40 kW high-power supply line, which may pose limitations. Conversely, the FJH process can provide transient 400 kW after being charged using the DC power supply of no more than 1 kW, making it highly suitable for laboratory environments. Therefore, while RJH is more appropriate for industrial production because of its controlled process, FJH is ideal for laboratory environments.

3.2. Effect of temperature on RG

To ascertain the optimal conditions to prepare graphene, carbon black was heated to 2600 °C, 3000 °C, and 3200 °C through RJH methods, denoted as RG-2600, RG-3000, and RG-3200, respectively.

The crystalline structure of RGs, as well as carbon black, was characterized using X-ray diffraction (XRD) (Fig. 4a). Compared to the broad (0 0 2) peak of carbon black, RG-2600, RG-3000 and RG-3200 exhibit a sharp (0 0 2) peak and a weak (1 0 0) peak and shift to higher angles, indicating complete graphitization of carbon black by the high-power RJH process. The calculated interlayer spacing of RG-2600, RG-3000 and RG-3200 was 0.347 nm, 0.343 nm, and 0.343 nm, respectively (Fig. 4b), larger than that of AB-stacked graphite (0.334 nm). In addition, all (0 0 2) peaks of RGs exhibit an asymmetrical shape, featuring a pronounced tail extending towards smaller angles. The characteristics mentioned above suggest that RGs possess a turbostratic structure similar to that reported for flash graphene [14,17,23].

High-quality graphene can be rapidly identified using Raman spectroscopy. The average Raman spectra of RGs and carbon black were collected from eight sample points (Fig. 4c). The D peak (~1354 cm^{-1}, breathing mode of sp^2-carbon atoms in rings), G peak (~1586 cm^{-1}, bond stretching of all pairs of sp2-carbon atoms in rings), and 2D peak (~2703 cm^{-1}, second-order zone boundary phonons in graphene) were observed simultaneously [24]. We assessed the quality of RG by analyzing the defect density using the intensity ratio of D peak to G peak (I_D/I_G), and the graphene conversion ratio using the intensity ratio of 2D peak to G peak (I_{2D}/I_G) (Fig. 4d). Among the three RG samples, RG-3000 exhibited the lowest I_D/I_G, indicating a low defect concentration in the graphene sheets. The smaller error bar of I_{2D}/I_G for RG-3000 also suggested its more uniform graphene structure [25,26]. In addition, the presence of TS$_1$ (~1861 cm^{-1}) and TS$_2$ (~1955 cm^{-1}) peaks and the absence of M peak (~1740 cm^{-1}) in RG-2600 and RG-3000 confirmed the turbostratic nature of RG (Fig. S5) [27]. While the presence of M peak in RG-3200 demonstrated that a high temperature exceeding 3000 °C can induce the graphene to stack in a more ordered structure. Therefore, 3000 °C is an optimal temperature for production of turbostratic graphene using the high-power RJH method.

Despite the relatively low energy consumption and high quality of RG, the high temperature of 3000 °C poses the primary challenge of RJH process. It is too high for the quartz tube, causing a layer of silicon
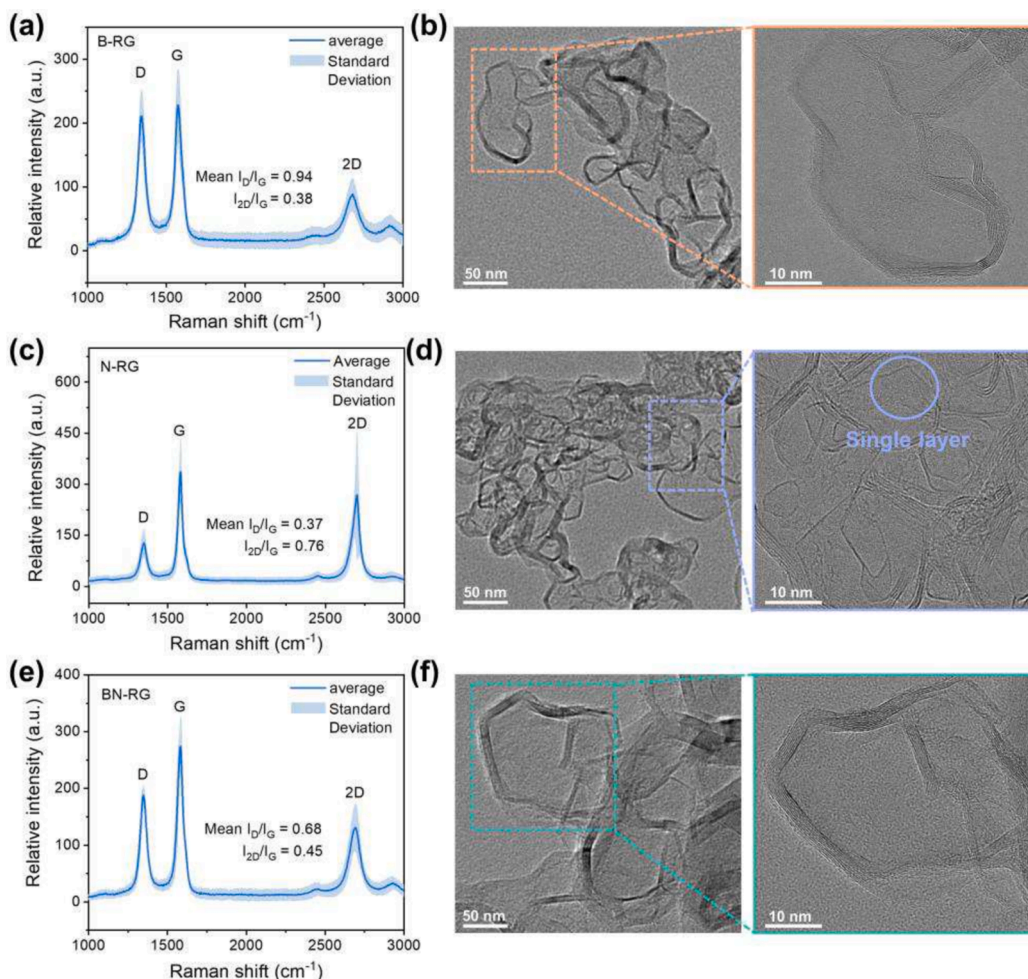
Fig. 5. Raman spectra (a, c, e), and TEM images (b, d, f) of B-RG, N-RG, and BN-RG.

carbide film to form on its inner surface. After undergoing approximately 5 RJH processes, the quartz tube became brittle and was subsequently discarded (Fig. S6). As a result, the cost of producing RG must factor in the expense of replacing these discarded quartz tubes. When factoring in the cost of these tubes, the overall cost of graphene production amounts to approximately $13 kg^{-1}, which includes the costs of raw carbon black at $2.5 kg^{-1}, energy at $0.5 kg^{-1}, and quartz tubes at $10.0 kg^{-1}. To reduce the cost of RG production, it is imperative to utilize tubes capable of withstanding high temperatures, such as boron nitride tubes, and/or to decrease the graphitization temperature through the use of catalytic additives, such as boron. If the cost associated with the tubes can be decreased to $1.0 kg^{-1}, thereby lowering the industrial production cost of graphene to $4 kg^{-1}, RG could potentially find widespread applications in various fields.

3.3. Mass production of doped graphene

Importantly, this high-power RJH method is also applicable for the low-cost mass production of doped graphene using various solid dopants. The raw materials of carbon black were mixed with 3 wt% B$_2$O$_3$ and 3 wt% melamine, either separately or together, to produce boron-doped RG (B-RG), nitrogen-doped RG (N-RG), and boron-nitrogen-co-doped RG (BN-RG), respectively. X-ray photoelectron spectroscopy (XPS) was employed to determine the chemical states of heteroatoms in doped RG. For B-RG, the atomic contents of carbon, oxygen, and boron were 97.08 %, 1.61 % and 1.31 %, respectively, confirming the successful doping of graphene with boron. The bonding types of boron

include B$_4$C [28], graphitic B (BC$_3$) [29], borinic B (C$_2$BO) [30], and boronic B (CBO$_2$) species (Fig. S7) [31]. For N-RG, only 0.38 wt% of nitrogen atoms was detected (Fig. S8), possibly due to the premature decomposition and volatilization of nitrogen source precursors during the heating process [32,33]. Additionally, dual doping can lead to graphene with high contents of heteroatoms, because it increases the bonding probability and mixing entropy. The atomic contents of carbon, oxygen, nitrogen, and boron in BN-RG were 94.71 %, 2.23 %, 1.84 % and 1.23 %, respectively, with the N content significantly higher than when using only N dopant alone (Fig. S9). The emerging bonding type of B-N indicated the co-doping effect of dual heteroatoms (Fig. S10).

Then we investigated the doping effect on the structural properties of RGs. The doping of boron reduces the interlayer distance of B-RG to 0.341 nm (Fig. S11), possibly due to the electronic deficiency-induced attraction caused by boron defects [34]. The interlayer distance of N-RG and BN-RG was 0.343 nm and 0.344 nm, respectively, which are similar to that of RG. The Raman spectra of B-RG show a high D peak and a low 2D peak (Fig. 5a), indicating that boron doping introduces more defects into the graphene lattice. As shown in the TEM images (Fig. 5b), B-RG is a polyhedron of multiple layers. In the Raman spectra of N-RG (Fig. 5c), the mean I_D/I_G intensity ratio is 0.37, even less than that of RG (0.44), indicating that slight N-doping does not increase the defects in graphene. Notably, the mean I_{2D}/I_G intensity ratio of N-RG is 0.76, significantly higher than that of RG (0.60). This implies that the average number of layers in N-RG is fewer than that in RG. TEM images further confirm there are some single-layer graphene sheets in N-RG, as highlighted by blue circle in Fig. 5d. In addition, the I_{2D}/I_G intensity ratio of
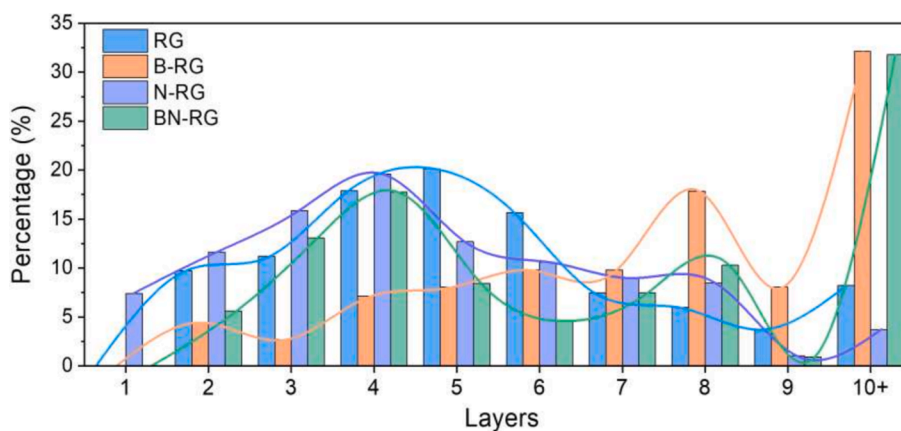
Fig. 6. Statistical distributions of number of layer of RG, B-RG, N-RG, and BN-NG.
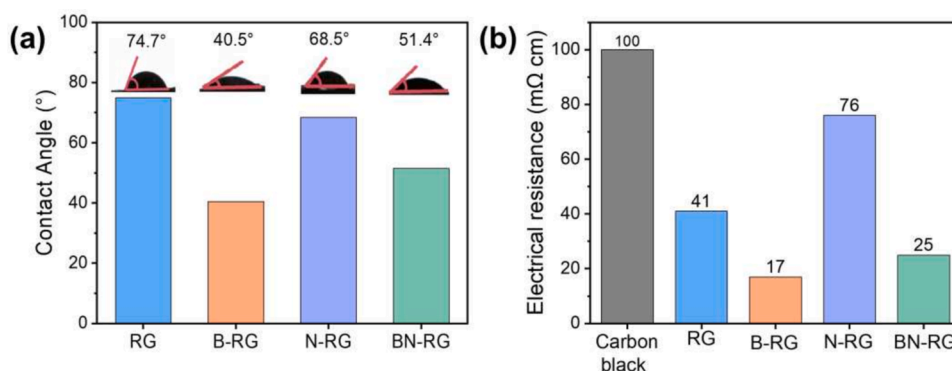

Fig. 7. Contact angles (a) and powder resistivity (b) of RG, B-RG, N-RG, and BN-NG.

BN-RG is between those of B-RG and N-RG (Fig. 5e), and its TEM images show some polyhedron multi-layered sheets similar to B-RG (Fig. 5f). Therefore, the crystal structure of BN-RG has intermediate characteristics of B-RG and N-RG.

The statistical distributions of number of layer of RG, B-RG, N-RG, and BN-NG, as counted from their TEM images, is shown in Figs. 6 and S12–15. The major thickness of RG, N-RG, and BN-RG is from 3 to 6 layers, while that of B-RG is from 4 to 8 layers. In particular, there are plenty of single- and double-layer sheets in N-RG. We believe that the decomposition and gasification of melamine at high temperatures can partly hinder the stacking of layers, resulting in thinner graphene sheets. In addition, approximately 30 % of the layers in B-RG and BN-RG are more than 10 layers thick. Consequently, in the high-power RJH process, the addition of melamine in carbon black can produce thinner graphene sheets, while the addition of boron can produce the thicker sheets.

3.4. Some physical properties of rapid graphene

The primary application of graphene powder is as an additive for reinforcing composite materials and enhancing conductivity [35–37]. To achieve optimal bonding with various substrates, the hydrophobicity of the graphene powder should align with the hydrophilicity or hydrophobicity of the substrate material. The contact angle of water is a measure of hydrophilicity or hydrophobicity, with a lower contact angle indicating higher hydrophilicity. The RG powder exhibits hydrophobicity with a contact angle of 74.7°, while the contact angles of N-RG, B-RG, and BN-RG decrease to 68.5°, 40.5°, and 51.4° (Fig. 7a), respectively. Heteroatom doping increases the polarity of graphene, thereby enhancing its hydrophilicity and making it suitable as a reinforcing additive in hydrophilic materials.

The electrical resistivity of RG powder was measured using a powder resistance tester under a pressure of 10 MPa. The graphitization process of RJH method converts amorphous carbon in carbon black into RG, resulting in a reduction of resistivity from 100 mΩ·cm to 41 mΩ·cm (Fig. 7b). Among all RGs, B-RG exhibited the lowest resistivity of 17 mΩ·cm, which may be attributed to the boron doping lowering the graphitization temperature and enhancing the structural integrity of the graphene sheets [34]. In contrast, nitrogen doping reduces the conductivity of graphene due to the smaller sizes of N-RG sheets, which increase contact resistance.

4. Conclusion

In this work, we developed a high-power RJH method for mass production of graphene with high yields. The high-power RJH process uses a scale-up Joule heating system by compressing 100 g of carbon black in a quartz tube, achieving temperatures up to 3000 °C in a few minutes. The process of transforming carbon black into graphene consists of pre-heating and graphitization phases, with an extremely low energy consumption of approximately 5 kWh per kilogram, which corresponds to a cost of $0.50 per kilogram. Theoretically, one device has the potential to generate as much as 5 tons of graphene per year. Additives like boron oxide and melamine are used for direct mass production of doped graphene. N-RG showed reduced sheet layers, while B-RG and BN-RG exhibited thicker sheets and increased conductivity. Consequently, these additives hold significant appeal for modifying the local structure and quality of RGs. Considering the extraordinary advantages of exceptional energy and time efficiency, decent product homogeneity, and structural modifiability, we anticipate that this high-power RJH method will have huge potential for the mass production

of graphene for industrial applications.

CRediT authorship contribution statement

Dan-Na Wu: Writing – original draft, Methodology, Investigation, Data curation, Conceptualization. **Jian Sheng:** Writing – review & editing, Data curation, Conceptualization. **Hai-Gang Lu:** Writing – review & editing, Supervision, Resources, Data curation. **Si-Dian Li:** Writing – review & editing. **Yan Li:** Writing – review & editing.

Declaration of competing interest

Acknowledgments

Appendix A. Supplementary data

Supplementary data to this article can be found online at https://doi.org/10.1016/j.cej.2025.159725.

Data availability

Data will be made available on request.

References

[1] A.K. Geim, K.S. Novoselov, The rise of graphene, Nat. Mater. 6 (2007) 183–191, https://doi.org/10.1038/nmat1849.

[2] K.S. Novoselov, A.K. Geim, S.V. Morozov, D. Jiang, Y. Zhang, S.V. Dubonos, I. V. Grigorieva, A.A. Firsov, Electric field effect in atomically thin carbon films, Science 306 (2004) 666–669, https://doi.org/10.1126/science.1102896.

[3] K.I. Bolotin, K.J. Sikes, Z. Jiang, M. Klima, G. Fudenberg, J. Hone, P. Kim, H. L. Stormer, Ultrahigh electron mobility in suspended graphene, Solid State Commun. 146 (2008) 351–355, https://doi.org/10.1016/j.ssc.2008.02.024.

[4] D.G. Papageorgiou, I.A. Kinloch, R.J. Young, Mechanical properties of graphene and graphene-based nanocomposites, Prog. Mater. Sci. 90 (2017) 75–127, https://doi.org/10.1016/j.pmatsci.2017.07.004.

[5] Z.W. Peng, R.Q. Ye, J.A. Mann, D. Zakhidov, Y.L. Li, P.R. Smalley, J. Lin, J.M. Tour, Flexible boron-doped laser-induced graphene microsupercapacitors, ACS Nano 9 (2015) 5868–5875, https://doi.org/10.1021/acsnano.5b00436.

[6] S. Agnoli, M. Favaro, Doping graphene with boron: a review of synthesis methods, physicochemical characterization, and emerging applications, J. Mater. 4 (2016) 5002–5025, https://doi.org/10.1039/c5ta10599d.

[7] T. Barkan, C.R. Ratwani, D. Johnson, K. Thodkar, C. Hill, Mapping the landscape for graphene commercialization, Nat. Rev. Phys. (2024), https://doi.org/10.1038/s42254-024-00754-9.

[8] L. Lin, H.L. Peng, Z.F. Liu, Synthesis challenges for graphene industry, Nat. Mater. 18 (2019) 520–524, https://doi.org/10.1038/s41563-019-0341-4.

[9] X.S. Li, W.W. Cai, J.H. An, S.Y. Kim, J. Nah, D.X. Yang, R. Piner, A. Velamakanni, I. Jung, E. Tutuc, S.K. Banerjee, L. Colombo, R.S. Ruoff, Large-area synthesis of high-quality and uniform graphene films on copper foils, Science 324 (2009) 1312–1314, https://doi.org/10.1126/science.1171245.

[10] D.C. Marcano, D.V. Kosynkin, J.M. Berlin, A. Sinitskii, Z.Z. Sun, A. Slesarev, L. B. Alemany, W. Lu, J.M. Tour, Improved synthesis of graphene oxide, ACS Nano 4 (2010) 4806–4814, https://doi.org/10.1021/nn1006368.

[11] Y.Y. Xu, H.Z. Cao, Y.Q. Xue, B. Li, W.H. Cai, Liquid-phase exfoliation of graphene: an overview on exfoliation media, techniques, and challenges, Nanomaterials 8 (2018) 942, https://doi.org/10.3390/nano8110942.

[12] A. Islam, B. Mukherjee, K.K. Pandey, A.K. Keshri, Ultra-fast, chemical-free, mass production of high quality exfoliated graphene, ACS Nano 15 (2021) 1775–1784, https://doi.org/10.1021/acsnano.0c09451.

[13] K.R. Paton, E. Varrla, C. Backes, R.J. Smith, U. Khan, A. O'Neill, C. Boland, M. Lotya, O.M. Istrate, P. King, T. Higgins, S. Barwich, P. May, P. Puczkarski, I. Ahmed, M. Moebius, H. Pettersson, E. Long, J. Coelho, S.E. O'Brien, E. K. McGuire, B.M. Sanchez, G.S. Duesberg, N. McEvoy, T.J. Pennycook, C. Downing, A. Crossley, V. Nicolosi, J.N. Coleman, Scalable production of large quantities of defect-free few-layer graphene by shear exfoliation in liquids, Nat. Mater. 13 (2014) 624–630, https://doi.org/10.1038/nmat3944.

[14] D.X. Luong, K.V. Bets, W.A. Algozeeb, M.G. Stanford, C. Kittrell, W.Y. Chen, R. V. Salvatierra, M.Q. Ren, E.A. McHugh, P.A. Advincula, Z. Wang, M. Bhatt, H. Guo, V. Mancevski, R. Shahsavari, B.I. Yakobson, J.M. Tour, Gram-scale bottom-up flash graphene synthesis, Nature 577 (2020) 647–651, https://doi.org/10.1038/s41586-020-1938-0.

[15] X.D. Zhu, L.T. Lin, M.Y. Pang, C. Jia, L.L. Xia, G.S. Shi, S.C. Zhang, Y.D. Lu, L. M. Sun, F.B. Yu, J. Gao, Z.L. He, X. Wu, A.D. Li, L. Wang, M.L. Wang, K. Cao, W. G. Fu, H.K. Chen, G. Li, J.B. Zhang, Y.J. Wang, Y. Yang, Y.G. Zhu, Continuous and low-carbon production of biomass flash graphene, Nat. Commun. 15 (2024) 3218, https://doi.org/10.1038/s41467-024-47603-y.

[16] L. Eddy, S.C. Xu, C.H. Liu, P. Scotland, W.Y. Chen, J.L. Beckham, B. Damasceno, C. H. Choi, K. Silva, A. Lathem, Y.M. Han, B.I. Yakobson, X.F. Zhang, Y.F. Zhao, J. M. Tour, Electric field effects in flash joule heating synthesis, J. Am. Chem. Soc. 146 (2024) 16010–16019, https://doi.org/10.1021/jacs.4c02864.

[17] M.G. Stanford, K.V. Bets, D.X. Luong, P.A. Advincula, W.Y. Chen, J.T. Li, Z. Wang, E.A. McHugh, W.A. Algozeeb, B.I. Yakobson, J.M. Tour, Flash graphene morphologies, ACS Nano 14 (2020) 13691–13699, https://doi.org/10.1021/acsnano.0c05900.

[18] L. Eddy, D.X. Luong, J.L. Beckham, K.M. Wyss, T.J. Cooksey, P. Scotland, C. H. Choi, W.Y. Chen, P.A. Advincula, Z.Y. Zhang, V. Mancevski, C. Kittrell, Y. M. Han, J.M. Tour, Automated laboratory kilogram-scale graphene production from coal, Small Methods 8 (2024) 2301144, https://doi.org/10.1002/smtd.202301144.

[19] Y.G. Yao, K.K. Fu, S.Z. Zhu, J.Q. Dai, Y.B. Wang, G. Pastel, Y.N. Chen, T. Li, C. W. Wang, T. Li, L.B. Hu, Carbon welding by ultrafast joule heating, Nano Lett. 16 (2016) 7282–7289, https://doi.org/10.1021/acs.nanolett.6b03888.

[20] Y.G. Yao, Z.N. Huang, P.F. Xie, S.D. Lacey, R.J. Jacob, H. Xie, F.J. Chen, A.M. Nie, T.C. Pu, M. Rehwoldt, D.W. Yu, M.R. Zachariah, C. Wang, R. Shahbazian-Yassar, J. Li, L.B. Hu, Carbothermal shock synthesis of high-entropy-alloy nanoparticles, Science 359 (2018) 1489–1494, https://doi.org/10.1126/science.aan5412.

[21] C.W. Wang, W.W. Ping, Q. Bai, H.C. Cui, R. Hensleigh, R.L. Wang, A.H. Brozena, Z. P. Xu, J.Q. Dai, Y. Pei, C.L. Zheng, G. Pastel, J.L. Gao, X.Z. Wang, H. Wang, J. C. Zhao, B. Yang, X.Y.R. Zheng, J. Luo, Y.F. Mo, B. Dunn, L.B. Hu, A general method to synthesize and sinter bulk ceramics in seconds, Science 368 (2020) 521–526, https://doi.org/10.1126/science.aaz7681.

[22] R.E. Franklin, Crystallite growth in graphitizing and non-graphitizing carbons, Proc. R. Soc. Lond. 209 (1951) 196–218, https://doi.org/10.1098/rspa.1951.0197.

[23] Z.Q. Li, C.J. Lu, Z.P. Xia, Y. Zhou, Z. Luo, X-ray diffraction patterns of graphite and turbostratic carbon, Carbon 45 (2007) 1686–1695, https://doi.org/10.1016/j.carbon.2007.03.038.

[24] L.M. Malard, M.A. Pimenta, G. Dresselhaus, M.S. Dresselhaus, Raman spectroscopy in graphene, Phys. Rep. 473 (2009) 51–87, https://doi.org/10.1016/j.physrep.2009.02.003.

[25] A.J. Pollard, B. Brennan, H. Stec, B.J. Tyler, M.P. Seah, I.S. Gilmore, D. Roy, Quantitative characterization of defect size in graphene using Raman spectroscopy, Appl. Phys. Lett. 105 (2014) 253107, https://doi.org/10.1063/1.4905128.

[26] A. Jorio, E.H. Martins Ferreira, M.V.O. Moutinho, F. Stavale, C.A. Achete, R. B. Capaz, Measuring disorder in graphene with the G and D bands, Phys. Status Solidi. 247 (2010) 2980–2982, https://doi.org/10.1002/pssb.201000247.

[27] J.A. Garlow, L.K. Barrett, L.J. Wu, K. Kisslinger, Y.M. Zhu, J.F. Pulecio, Large-area growth of turbostratic graphene on Ni (111) via physical vapor deposition, Sci. Rep. 6 (2016) 19804, https://doi.org/10.1038/srep19804.

[28] W. Cermignani, T.E. Paulson, C. Onneby, C.G. Pantano, Synthesis and characterization of boron-doped carbons, Carbon 33 (1995) 367–374, https://doi.org/10.1016/0008-6223(94)00160-2.

[29] T. Shirasaki, A. Derré, M. Ménétrier, A. Tressaud, S. Flandrois, Synthesis and characterization of boron-substituted carbons, Carbon 38 (2000) 1461–1467, https://doi.org/10.1016/s0008-6223(99)00279-1.

[30] S. Jacques, A. Guette, X. Bourrat, F. Langlais, C. Guimon, C. Labrugere, LPCVD and characterization of boron-containing pyrocarbon materials, Carbon 34 (1996) 1135–1143, https://doi.org/10.1016/0008-6223(96)00075-9.

[31] T.V. Khai, H.G. Na, D.S. Kwak, Y.J. Kwon, H. Ham, K.B. Shim, H.W. Kim, Comparison study of structural and optical properties of boron-doped and undoped graphene oxide films, Chem. Eng. J. 211 (2012) 369–377, https://doi.org/10.1016/j.cej.2012.09.081.

[32] W.Y. Chen, C. Ge, J.T. Li, J.L. Beckham, Z. Yuan, K.M. Wyss, P.A. Advincula, L. Eddy, C. Kittrell, J.H. Chen, D.X. Luong, R.A. Carter, J.M. Tour, Heteroatom-doped flash graphene, ACS Nano 16 (2022) 6646–6656, https://doi.org/10.1021/acsnano.2c01136.

[33] S. Zhu, F. Zhang, H.G. Lu, J. Sheng, L.N. Wang, S.D. Li, G.Y. Han, Y. Li, Flash nitrogen-doped graphene for high-rate supercapacitors, ACS Mater. Lett. 4 (2022) 1863–1871, https://doi.org/10.1021/acsmaterialslett.2c00616.

[34] A. Ōya, R. Yamashita, S. Ōtani, Catalytic graphitization of carbons by borons, Fuel 58 (1979) 495–500, https://doi.org/10.1016/0016-2361(79)90167-4.

[35] P.A. Advincula, W. Meng, L.J. Eddy, J.L. Beckham, I.R. Siqueira, D.X. Luong, W. Y. Chen, M. Pasquali, S. Nagarajaiah, J.M. Tour, Ultra-high loading of coal-derived

flash graphene additives in epoxy composites, Macromol. Mater. Eng. 308 (2023) 2200640, https://doi.org/10.1002/mame.202200640.

[36] P.A. Advincula, V. Granja, K.M. Wyss, W.A. Algozeeb, W.Y. Chen, J.L. Beckham, D. X. Luong, C.F. Higgs, J.M. Tour, Waste plastic-and coke-derived flash graphene as lubricant additives, Carbon 203 (2023) 876–885, https://doi.org/10.1016/j. carbon.2022.12.035.

[37] B.S. Damasceno, A.F.V.D. Silva, L. Eddy, A.N.D. Melo, J.L. Beckham, C.H. Choi, Y. M. Han, J.M. Tour, A.C.V.D. Araújo, G.P. Thim, A.S.D. Silva Sobrinho, A.L.D. J. Pereira, D.M.G. Leite, Flash graphene and poly (o-methoxy aniline) for the composition of a solvent-based conductive ink, Surf. 50 (2024) 104427, https://doi.org/10.1016/j.surfin.2024.104427.